Supplement of Aerosol Research, 4, 169–187, 2026
https://doi.org/10.5194/ar-4-169-2026-supplement

AEROSOL Research
Open Access

Supplement of

Characterizing aerosol sources based on aerosol optical properties and dispersion modelling in a Scandinavian Coastal Area (Aarhus, Denmark)

Zihui Teng et al.

Correspondence to: Bernadette Rosati (bernadette.rosati@boku.ac.at)

- BC source apportionment
- Figure S1: Schematic of instrumental setup at the measurement site.
- Figure S2: Inlet and sampling probe efficiency curves.
- Figure S3: Ångström matrix for entire campaign colour-coded by single scattering albedo at 520 nm.
- Figure S4: Diurnal variation median value of σ_{sca} at 525 nm and median values of σ_{abs} at 520 nm at different weeks.
- Figure S5: Radiation time during a day throughout the campaign.
- Figure S6: Diurnal variation of median radiation time each hour.
- Figure S7: FLEXPART source contributions to black carbon concentrations.
- Figure S8: FLEXPART emission sensitivity for black carbon for the three selected case periods.
- Figure S9: CO, PM_{10}, and NO_x concentration throughout the campaign.
- Figure S10: Wind speed and direction throughout the campaign.
- Figure S11: Case 1: NO_x, CO and eBC_{AE33} concentrations.
- Figure S12: Case 1: FLEXPART continental contributions to black carbon concentrations.
- Figure S13: Case 1: Particle number and surface size distributions.
- Figure S14: Case 2: NO_x, CO and eBC_{AE33} concentrations.
- Figure S15: Case 2: Particle number and surface size distributions.
- Figure S16: Case 3: NO_x, CO and eBC_{AE33} concentrations.
- Figure S17: Case 3: Particle number and surface size distributions.
- Figure S18: FLEXPART age spectrum for black carbon concentrations for entire campaign.

Black carbon source apportionment

Black carbon source apportionment was performed as proposed in Sandradewi et al. (2008). This method is based on the assumption that absorption is caused by particle matter from biomass burning and combustion of fossil fuels. It applies absorption Ångström exponents of fossil fuel combustion and biomass burning of α_{ff} = 1 for fossil fuel and α_{bb} = 2 for biomass. These values were used in our calculations as no axillary measurements (such as EC/OC data or ^{14}C, see e.g. Sandradewi et al., 2008; Zotter et al., 2017), were available. The absorption coefficient at 470 and 950 nm is used, along with the fixed exponents, to calculate the contributions from fossil fuel and biomass burning. In this formula, $b_{abs}(\lambda)$ is the absorption coefficient at a certain wavelength λ, *ff* indicates contribution from fossil fuel, and *bb* indicates the contribution from biomass burning.

$$\frac{b_{\mathrm{abs,ff}}(470\,\mathrm{nm})}{b_{\mathrm{abs,ff}}(950\,\mathrm{nm})} = \left(\frac{470}{950}\right)^{-\alpha_{\mathrm{ff}}} \tag{S1}$$

$$\frac{b_{\mathrm{abs,bb}}(470\,\mathrm{nm})}{b_{\mathrm{abs,bb}}(950\,\mathrm{nm})} = \left(\frac{470}{950}\right)^{-\alpha_{\mathrm{bb}}} \tag{S2}$$

$$b_{\mathrm{abs}}(470\,\mathrm{nm}) = b_{\mathrm{abs,bb}}(470\mathrm{nm}) + b_{\mathrm{abs,ff}}(470\mathrm{nm}) \tag{S3}$$

$$b_{\mathrm{abs}}(950\,\mathrm{nm}) = b_{\mathrm{abs,bb}}(950\mathrm{nm}) + b_{\mathrm{abs,ff}}(950\mathrm{nm}) \tag{S4}$$

While Fraction of biomass burning BB% of black carbon is calculated by:

$$BB\% = \frac{b_{\mathrm{abs,bb}}(950\mathrm{nm})}{b_{\mathrm{abs}}(950\mathrm{nm})} \tag{S5}$$

The mass concentration of BC from biomass burning is calculated by multiplying the BC at 880 nm by the BB% and BC$_{ff}$ is calculated from the total BC substrate contributed by biomass burning.

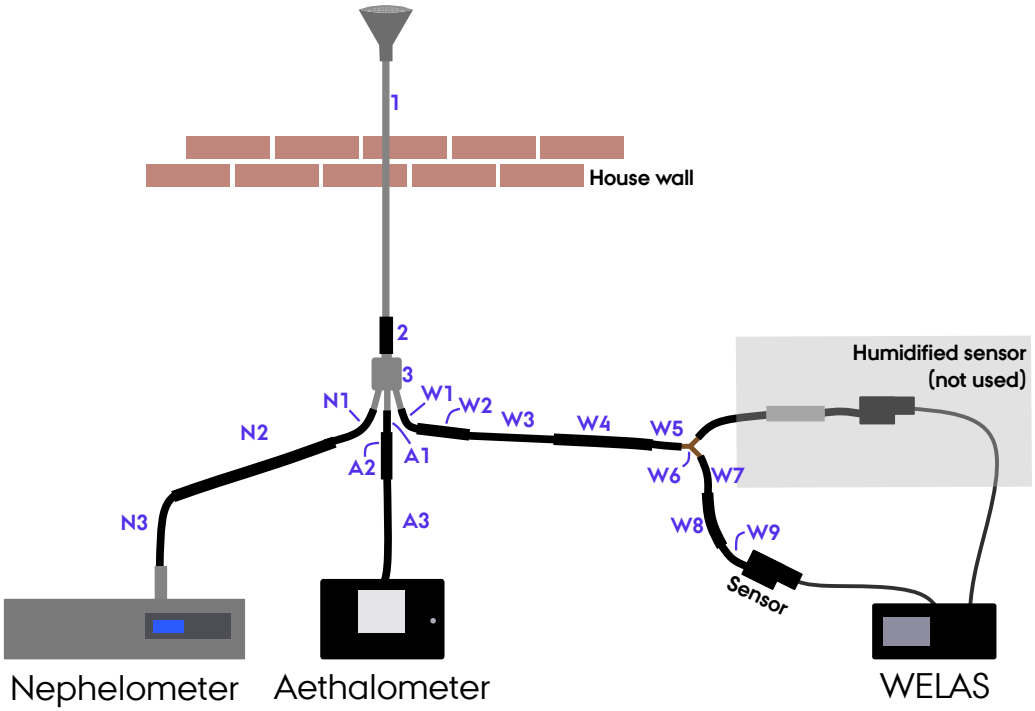

Figure S1: Schematic of the instrumental setup at the measurement site showing the sampling probe, tubing and instruments. Tubing lengths, angle of inclination, and angle of curvatures are not drawn to scale and are intended only for illustrative purposes. 1-3 are the inlet tubes. N1-N3 depict tubing to the nephelometer, A1-A3 to the aethalometer and W1-W9 to the WELAS. The indicated humidified part was not used for the analysis due to technical issues.

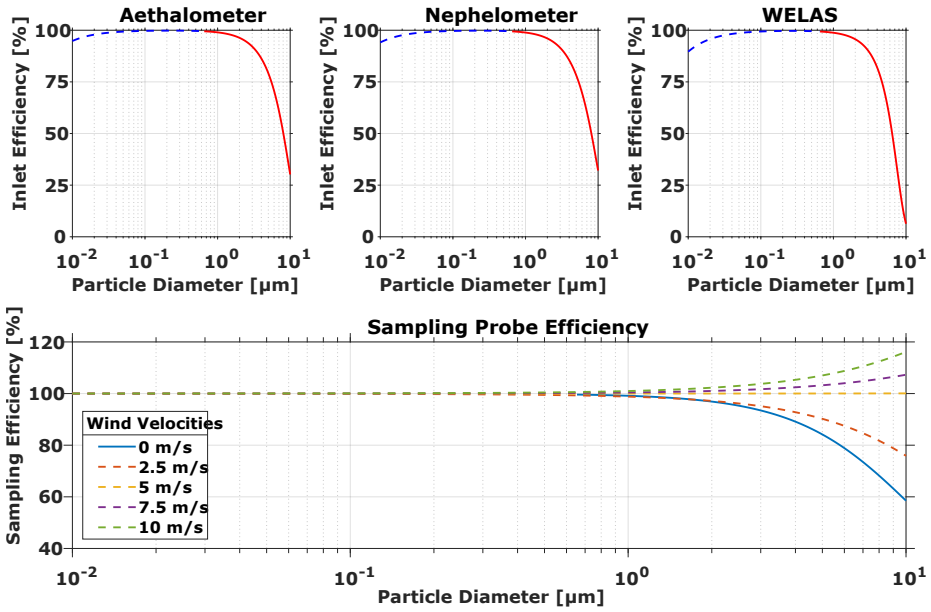

Figure S2: Upper panels: Inlet efficiency curves calculated for each instrument: aethalometer, nephelometer, and WELAS. Lower panel: Sampling probe efficiency curves at different wind velocities. Dashed lines indicate an approximation, as one or more of the formulas in the particle loss calculator are outside their validation limit von der Weiden et al. (2009). Solid lines indicate all formulas are within their stated validity range.

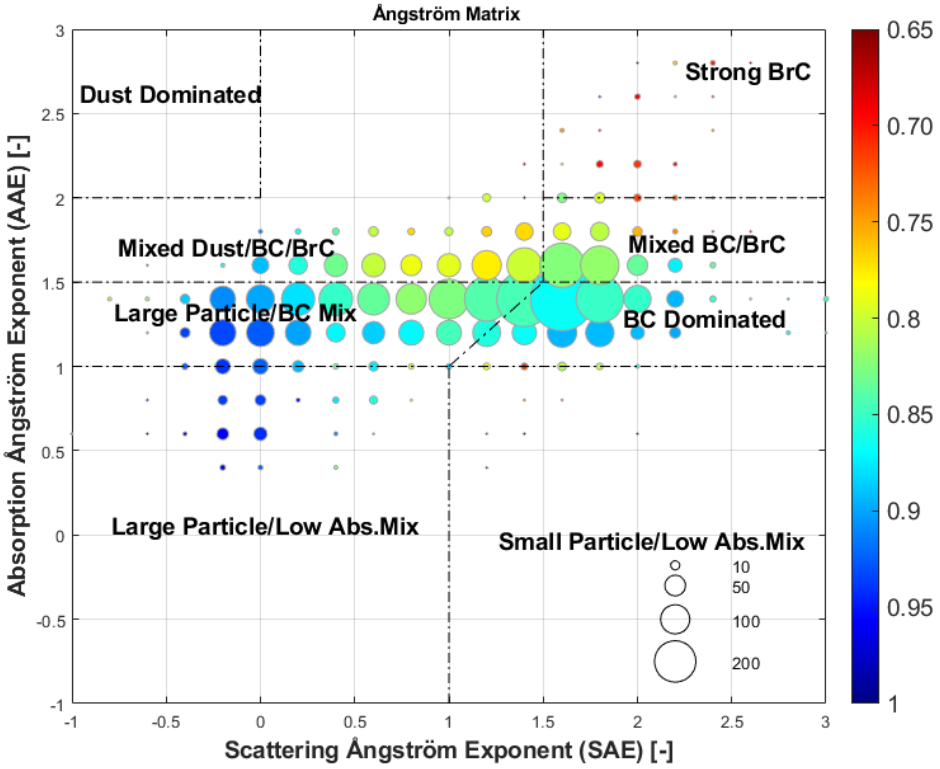

Figure S3: Ångström matrix colour-coded by single scattering albedo at 520 nm for the entire campaign.The SAE and AAE values were binned using a bin-width of 0.2. Data was averaged for 10 min. The size of the circles denotes the number of data points within each bin.

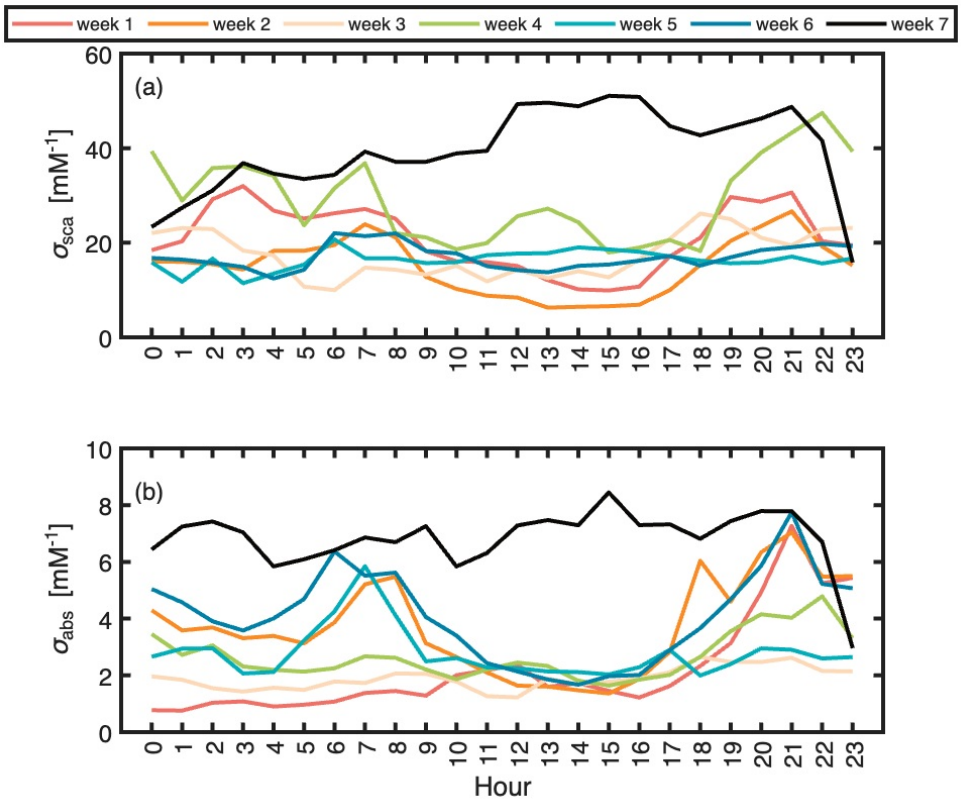

Figure S4: Diurnal variation of (a) median value of σ_{sca} at 525 nm and (b) median values of σ_{abs} at 520 nm grouped by calender week (Monday-Sunday) during the measurement period (3 March-11 April). Each line represents one calender week; weeks may not contain complete data coverage for all days

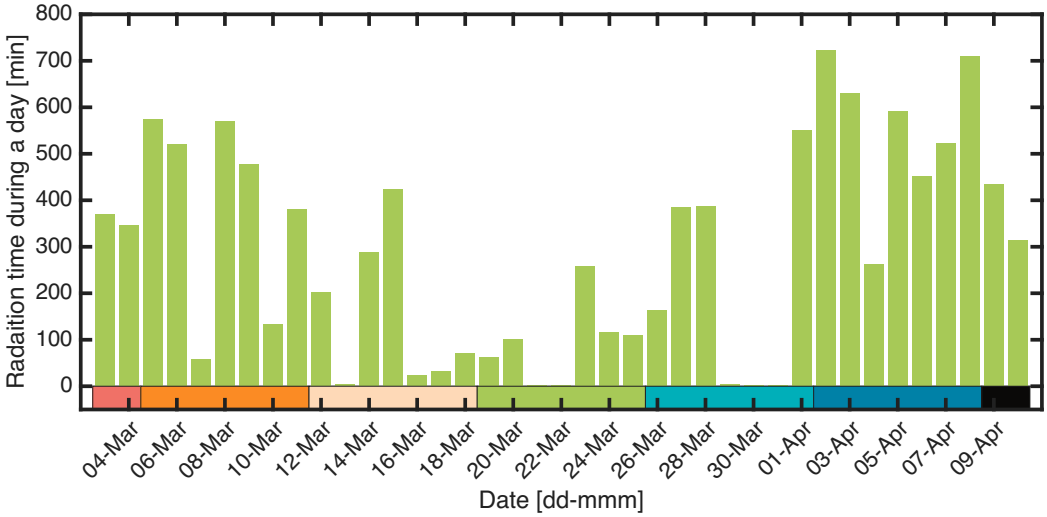

Figure S5: Radiation time each day from 3 March to 4 April 2023.

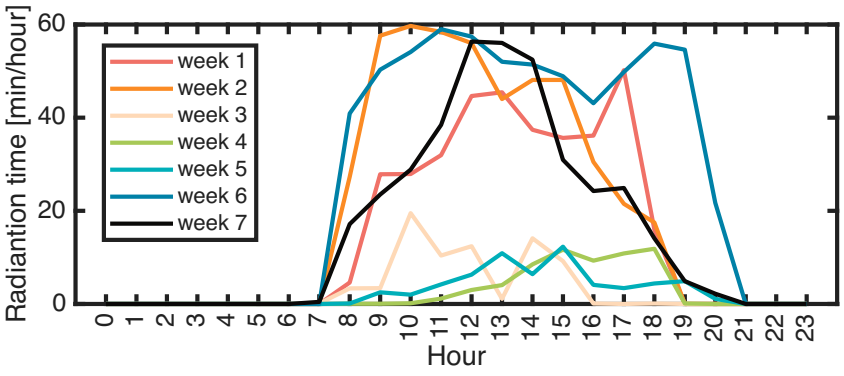

Figure S6: Diurnal variation of median radiation time each hour during different weeks (colored lines).

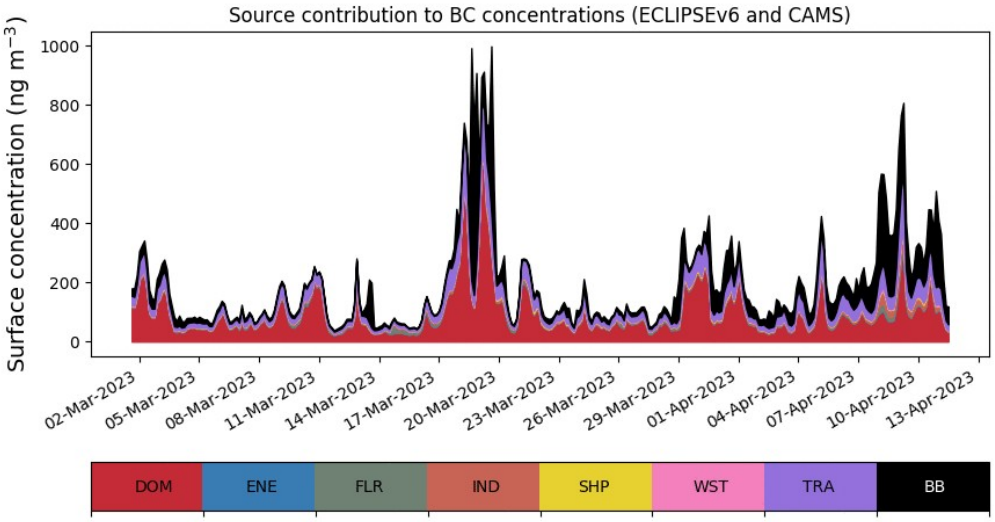

Figure S7: FLEXPART source contributions to black carbon concentrations during the entire measurement period. Emissions from industrial combustion (IND), from the energy production sector (ENE), residential and commercial emissions (DOM), waste treatment and disposal sector (WST), transportation (TRA), shipping activities (SHP), gas flaring emissions (FLR), and biomass burning (BB) from wildfires.

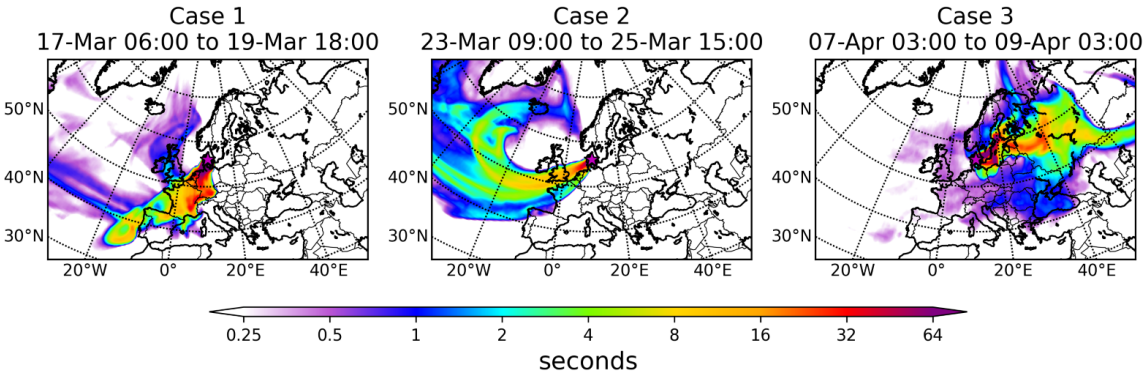

Figure S8: FLEXPART footprint: emission sensitivity for black carbon for Case 1, Case 2, and Case 3.

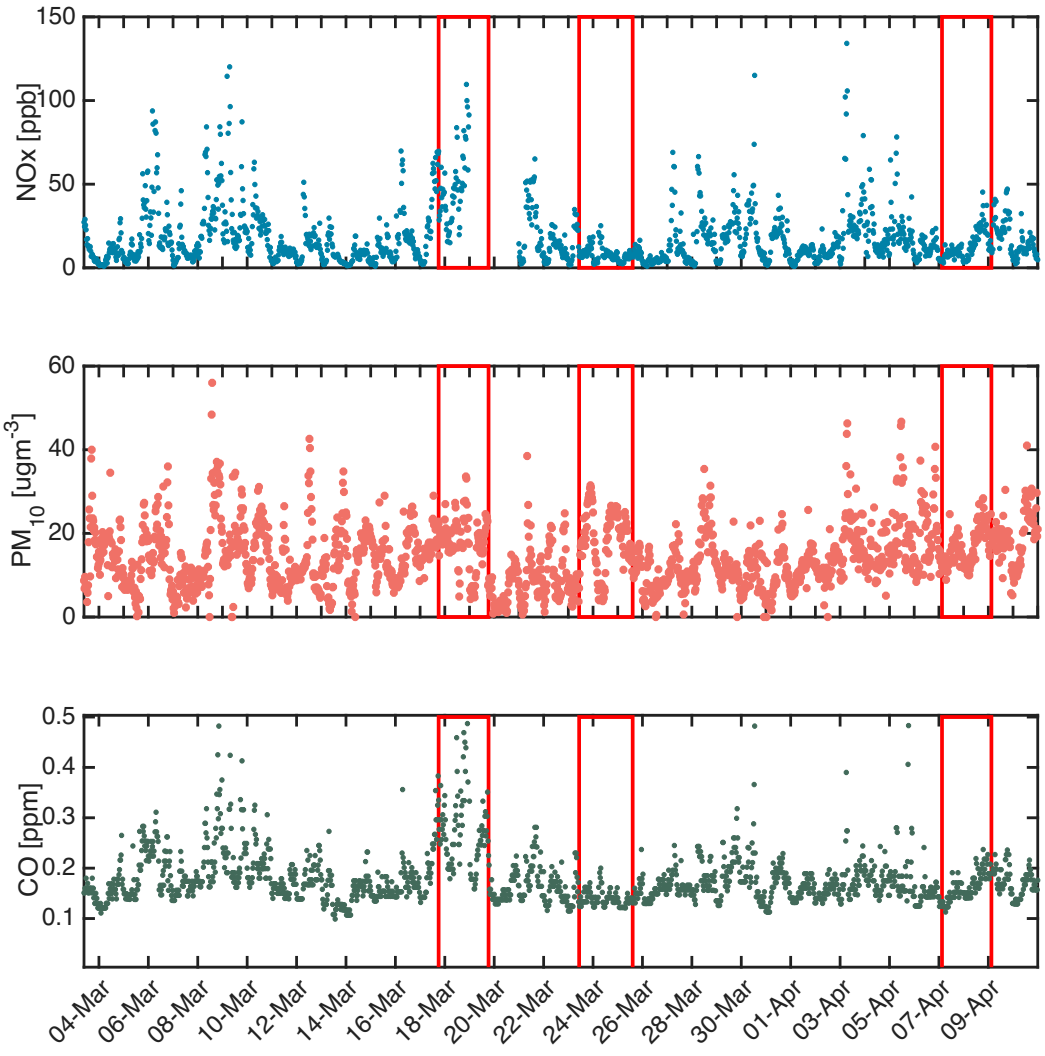

Figure S9: CO, PM_{10}, and NO_x data from DCE station. Case 1, Case 2, and Case 3 are highlighted with red squares.

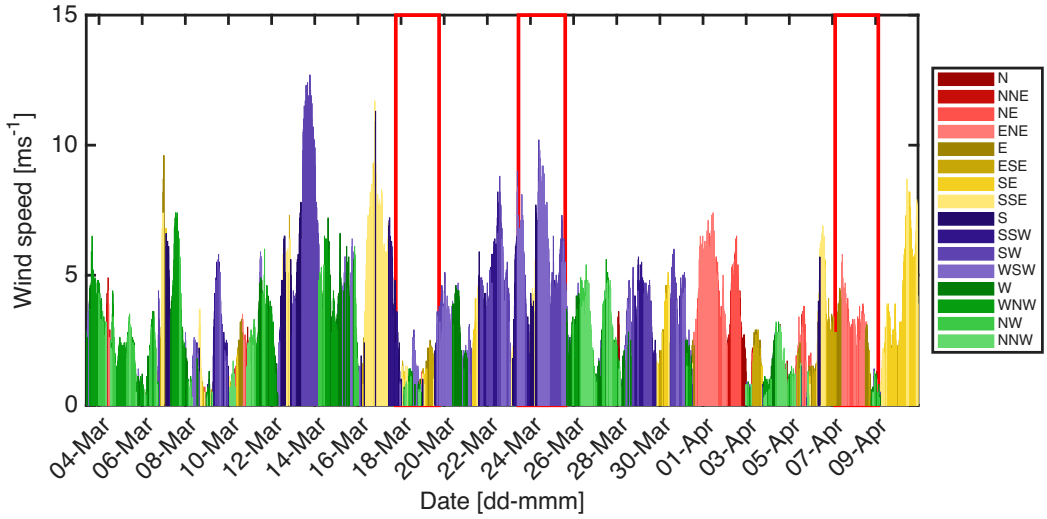

Figure S10: Wind speed, colour-coded by wind direction, from 3 March to 4 April 2023. Case 1, Case 2, and Case 3 are highlighted with red squares.

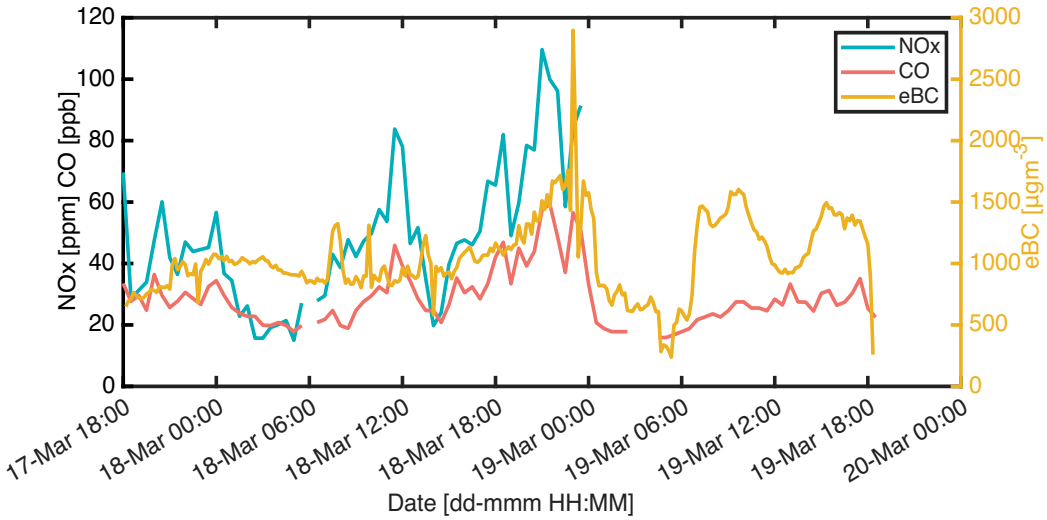

Figure S11: Case 1: Time series of NO_x, CO and eBC_{AE33} concentrations.

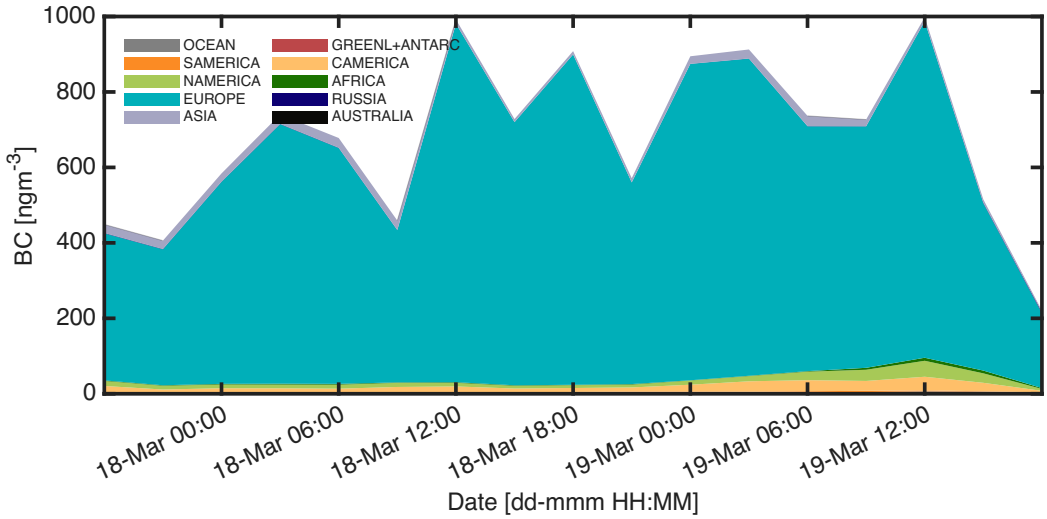

Figure S12: Case 1: FLEXPART continental contributions to black carbon concentrations.

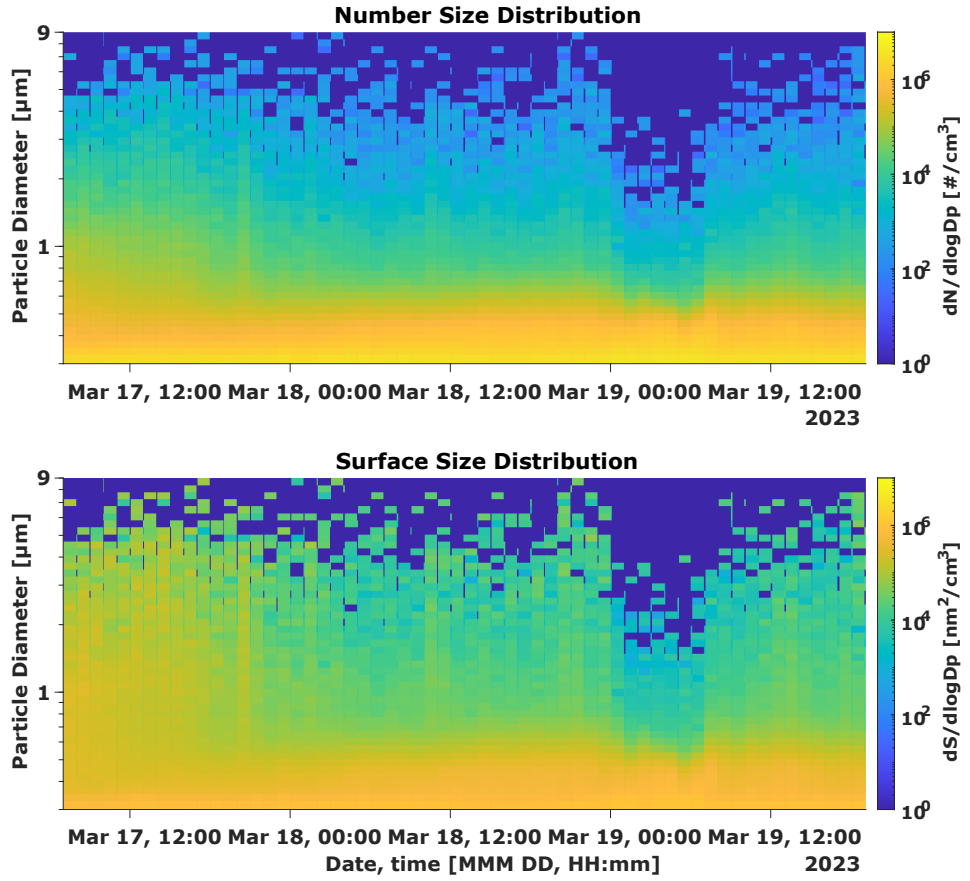

Figure S13: Case 1: Particle number and surface size distributions.

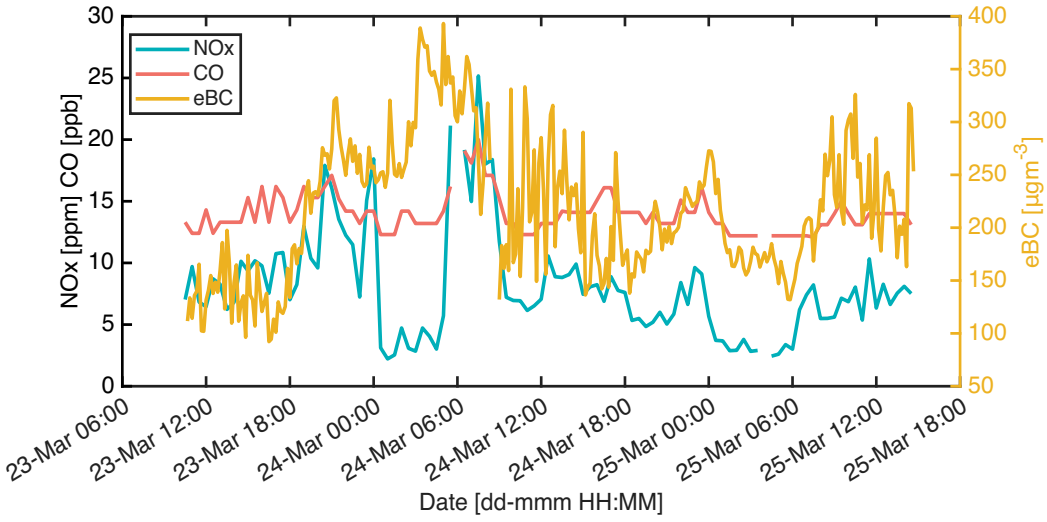

Figure S14: Case 2: Time series of NO_x, CO and eBC_{AE33} concentrations during.

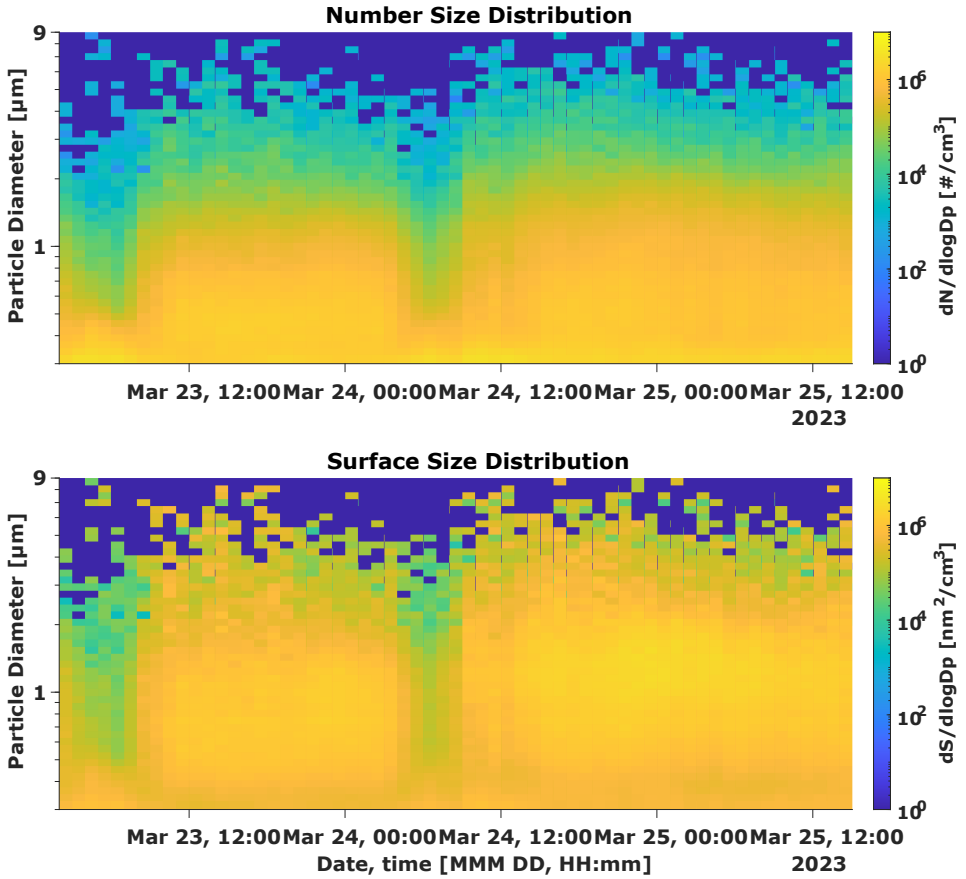

Figure S15: Case 2: Particle number and surface size distributions.

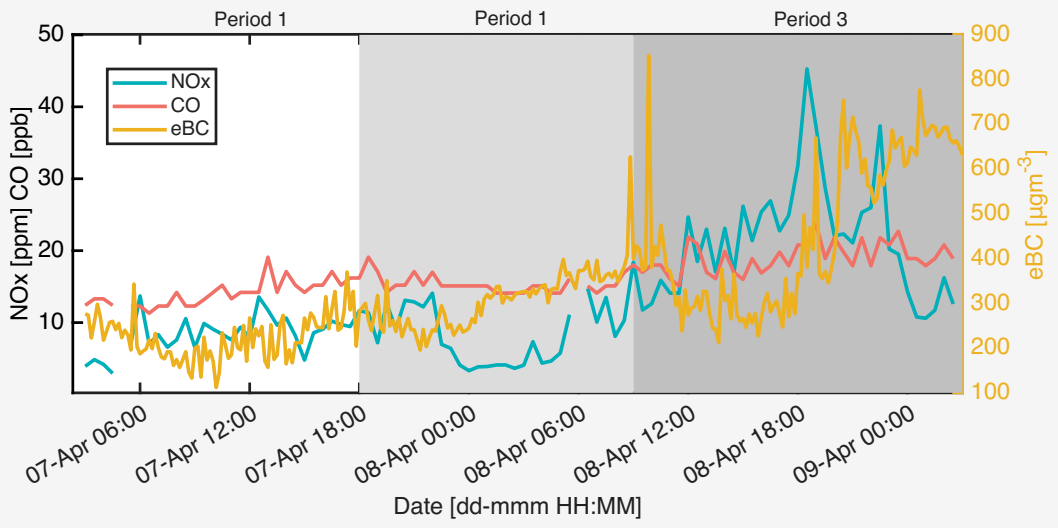

Figure S16: Case 3: Time series of NO_x, CO and eBC_{AE33} concentrations during.

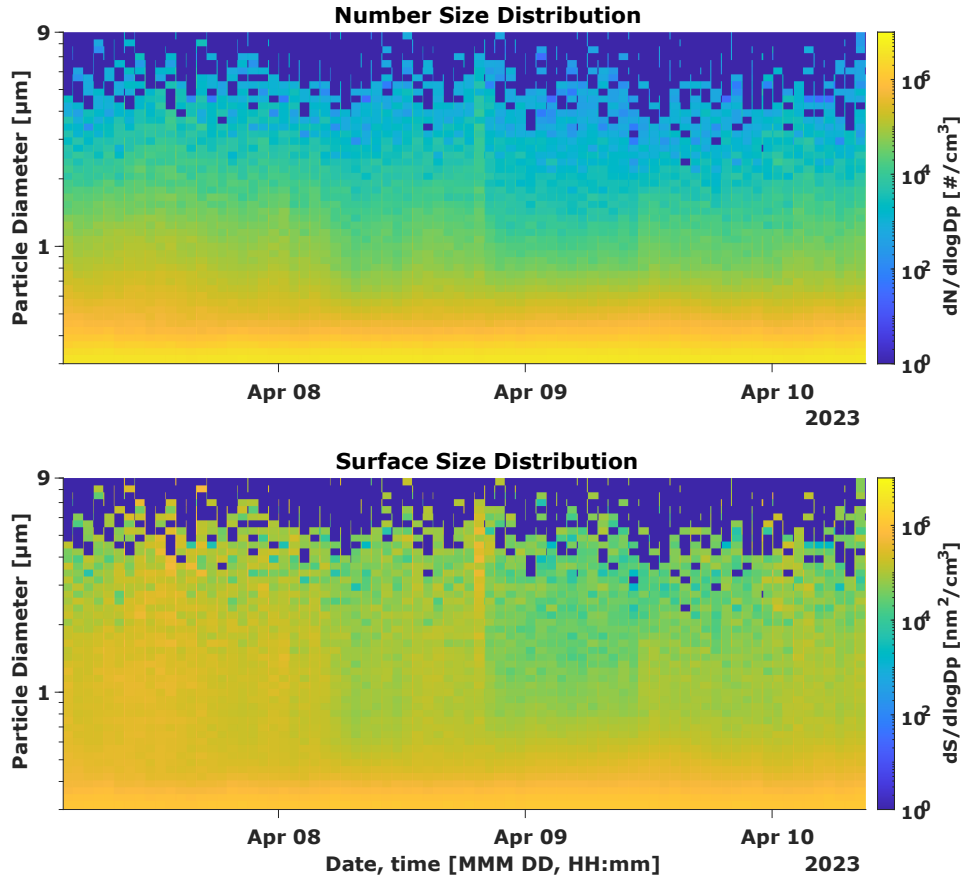

Figure S17: Case 3: Particle number and surface size distribution.

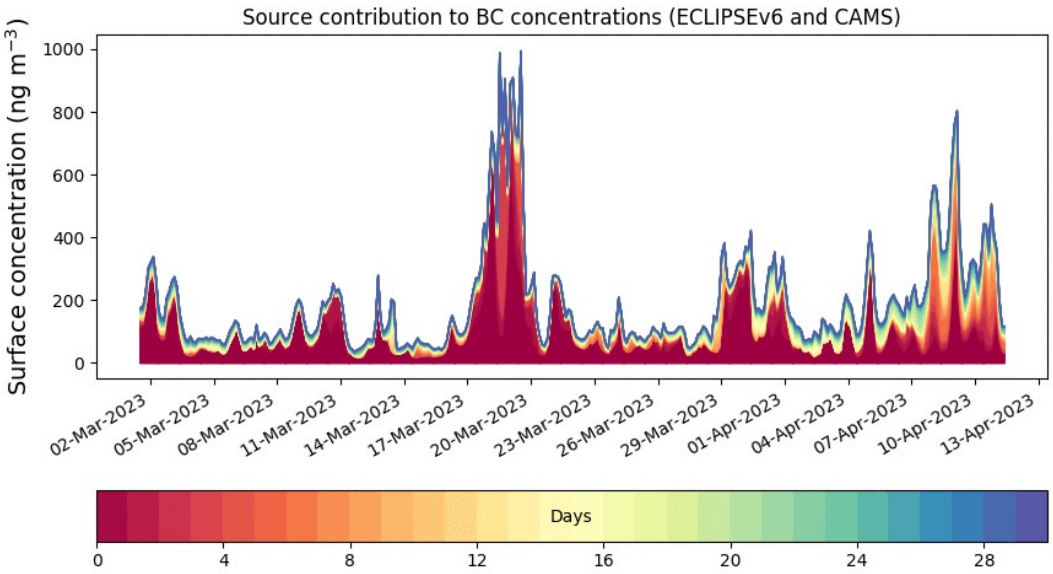

Figure S18: FLEXPART age spectrum for black carbon concentrations for the entire campaign.

Table S1: Tubing parameters for each tubing piece leading to the nephelometer. See schematic of inlet, tubing, and instruments in Fig. S1. Diameter A and B refer to inner diameter at each end of the tube. Inclination (incl.) angle is the angle the tube is inclined with respect to horizontal and curvature (curv.) angle is the angle of curvature of the bend of the tube von der Weiden et al. (2009).

Tube #	**Flow rate (L/min)**	**Length (m)**	**Diam A (nm)**	**Diam B (nm)**	**Incl. angle (°)**	**Curv. angle (°)**
1	15	0.37	8	8	0	0
2	15	0.02	8	8	0	40
3	15	0.05	8	6	40	0
N1	5	0.115	6	6	40	0
N2	5	0.25	8	8	40	0
N3	5	0.17	12	12	40	50

Table S2: Tubing parameters for each tubing piece leading to the aethalometer. See schematic of inlet, tubing, and instruments in Fig. S1. Diameter A and B refer to inner diameter at each end of the tube. Inclination (incl.) angle is the angle the tube is inclined with respect to horizontal and curvature (curv.) angle is the angle of curvature of the bend of the tube von der Weiden et al. (2009).

Tube #	**Flow rate (L/min)**	**Length (m)**	**Diam A (nm)**	**Diam B (nm)**	**Incl. angle (°)**	**Curv. angle (°)**
1	15	0.37	8	8	0	0
2	15	0.02	8	8	0	40
3	15	0.05	8	6	40	0
A1	5	0.052	6	6	40	0
A2	5	0.057	8	8	40	20
A3	5	0.412	6	6	60	20

Table S3: Tubing parameters for each tubing piece leading to the WELAS. See schematic of inlet, tubing, and instruments in Fig. S1. Diameter A and B refer to inner diameter at each end of the tube. Inclination (incl.) angle is the angle the tube is inclined with respect to horizontal and curvature (curv.) angle is the angle of curvature of the bend of the tube von der Weiden et al. (2009).

Tube #	**Flow rate (L/min)**	**Length (m)**	**Diam A (nm)**	**Diam B (nm)**	**Incl. angle (°)**	**Curv. angle (°)**
1	15	0.37	8	8	0	0
2	15	0.02	8	8	0	40
3	15	0.05	8	6	40	0
W1	5	0.043	6	6	40	0
W2	5	0.126	8	8	40	0
W3	5	0.31	6	6	40	100
W4	5	0.285	8	8	20	20
W5	5	0.05	6	6	40	0
W6	5	0.02	6	6	40	120
W7	5	0.1	6	6	50	30
W8	5	0.08	8	8	80	10
W9	5	0.1	6	6	90	0

Bibliography

Sandradewi, J., Prevot, A., Szidat, S., Perron, N., Alfarra, M., Lanz, V., Weingartner, E., and Baltensperger, U. (2008). Using aerosol light absorption measurements for the quantitative determination of wood burning and traffic emission contributions to particulate matter. *Environmental science & technology*, 42:3316–23.

von der Weiden, S.-L., Drewnick, F., and Borrmann, S. (2009). Particle loss calculator – a new software tool for the assessment of the performance of aerosol inlet systems. *Atmospheric Measurement Techniques*, 2(2):479–494.

Zotter, P., Herich, H., Gysel, M., El-Haddad, I., Zhang, Y., Močnik, G., Hüglin, C., Baltensperger, U., Szidat, S., and Prévôt, A. S. H. (2017). Evaluation of the absorption ångström exponents for traffic and wood burning in the aethalometer-based source apportionment using radiocarbon measurements of ambient aerosol. *Atmospheric Chemistry and Physics*, 17(6):4229–4249.